DOI: 10.31401/WS.2024.proc.02

The Backreaction of the Reduced Heliospheric Pressure on CMEs and Its Implications for the Strength of Solar Cycle 25

Gopalswamy N.[1], *Akiyama S.*[1,2], *Yashiro S.*[1,2], *Mäkelä P.*[1,2], *Xie H.*[1,2], *Michalek G.*[3]

[1]NASA Goddard Space Flight Center, Maryland, USA; nat.gopalswamy@nasa.gov
[2]The Catholic University of America, Washington DC, USA
[3]Jagiellonian University, Krakow, Poland

Abstract

We investigated the abundance of halo coronal mass ejections (CMEs), solar flares, and solar wind conditions that occurred during the first 49 months of solar cycles 23-25. We find that the halo CME abundance has an inverse relation with the solar cycle strength. The reduced heliospheric total pressure, whose backreaction on CMEs allows them to expand more, resulted in the higher halo CME abundance in the weaker cycle 24. This trend continues in cycle 25, indicating that this cycle is also weak. Related effects in weaker cycles are the wider longitudinal distribution of halo CME sources and the halo formation closer to the Sun at lower CME speeds. The size of soft X-ray flares is similar and the flare abundance is not significantly different in the three cycles, indicating that the weakened state of the heliosphere affects CMEs, but not flares. These results imply that cycle 25 is weaker than cycle 23 but similar in strength to cycle 24.

Keywords: Heliospheric pressure; Halo coronal mass ejections; Solar cycle prediction.

Introduction

The backreaction of the heliospheric pressure on the properties of coronal mass ejections (CMEs) was first recognized as the anomalous expansion of CMEs during the maximum phase of solar cycle (SC) 24 (Gopalswamy et al. 2014). While the width and speed of CMEs were well correlated as in SC 23, the slope of the speed-width relationship significantly increased in SC 24. The heliospheric backreaction has been found to manifest in many ways, including (i) enhanced halo CME abundance (Gopalswamy et al. 2015a: Dagnew et al. 2020a), (ii) halo formation closer to the Sun at lower CMEs speeds (Gopalswamy et al. 2022), (iii) wider longitudinal distribution of halo CMEs (Gopalswamy et al. 2015), (iv) change in slope of the CME expansion speed – CME radial speed relationship (Dagnew et al. 2020b), and (v) larger pressure balance distance for CME flux ropes (Gopalswamy et al. 2015b; Dagnew et al. 2022). The current SC 25 is in its maximum phase and has witnessed a significant number of CMEs in the first 4 years since its beginning in December 2019, providing an opportunity to test the heliospheric backreaction on CMEs and assess the strength of the cycle. Such an assessment is important in discriminating the widely varying predictions of the strength of SC 25 that vary from a sunspot number of 50 to >200 (Nandy 2021). Furthermore, using SC 25 data is important in confirming the results obtained by comparing just two SCs. In this paper, we revisit the properties of halo CMEs that occurred during SCs 23-25 and show that SC 25 is indeed weak, similar to SC 24 but slightly stronger (Gopalswamy et al. 2018; 2022; Bhowmik et al. 2018). Therefore, the space weather in SC 25 is expected to be milder than in SC 23.

Halo CME Observations

Halo CMEs observed by a given coronagraph discriminate energetic CMEs that expand rapidly early on, so they appear to surround the occulting disk (Howard et al. 1982; 1985; Zhao and Webb 2003; Gopalswamy et al. 2010). Halo CMEs are key players in space weather owing to their high energy and their direction of propagation close to the Sun-Earth line (Gopalswamy 2009; Zhang et al. 2021; Gopalswamy 2022). We make use of the halo CMEs manually identified, cataloged, and made available online at NASA's CDAW Data Center (https://cdaw.gsfc.nasa.gov) with added information from the general CME catalog (Yashiro et al. 2004; Gopalswamy et al. 2009; 2024). Halo CMEs are identified in the coronagraph images obtained by the Large Angle Spectrometric Coronagraphs (LASCO, Brueckner et al. 1995) on board the Solar and Heliospheric Observatory (SOHO, Domingo et al. 1995).

Comparing halo CMEs in SCs 23 and 24 up to the maximum phase, Gopalswamy et al. (2015a) found that the halo CME abundance was higher in SC 24, even though the average sunspot number (SSN) declined by ~40%. The halo CME abundance was defined as the number of halo CMEs observed over a certain time interval divided by the daily SSN averaged over the same interval. Dagnew et al. (2020a) compared halo CMEs over the whole SCs 23 and 24 and confirmed the increase in halo CME abundance by ~44%, while the average SSN declined by ~46%. Here we compare the halo CME abundance over the first 49 months of SCs 23-25. The halo CME catalog (https://cdaw.gsfc.nasa.gov/, Gopalswamy et al. 2010) lists more than 800 halos since 1996. Figure 1 shows the semiannual variation of the number of halos in comparison with SSN. We see that the halo CME variation is in phase with the SSN variation, but the amplitudes are quite different. Such variation has also been found in the general population of CMEs as well (Petre 2015; Michalek et al. 2019). There were 100, 137, and 144 halos observed during the first 49 months of SCs 23, 24, and 25, respectively. We compare these numbers with respect to the average SSNs during these intervals.

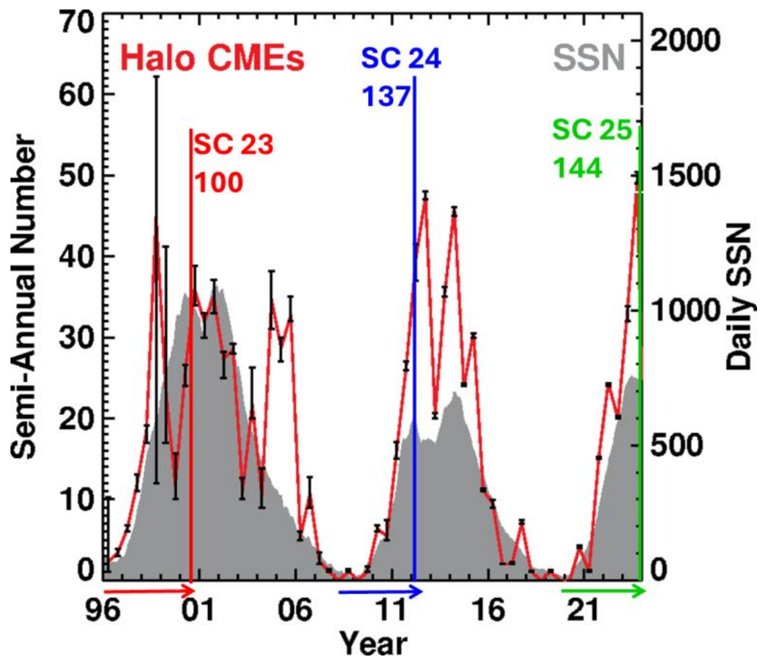

***Figure 1**. Semi-annual variation of the number of halo CMEs as a function of time since 1996 until the end of 2023. The daily SSN from SILSO (Sunspot Index and Long-term Solar Observations, **http://www.sidc.be/silso**) is shown for comparison. The arrows marked at the bottom of the plot indicate equal time intervals (49 months) from the beginning of each SC. The number of halos observed in these intervals are noted on the plot. The error bars are based on the data gaps in SOHO/LASCO observations.*

a. Halo CME abundances

Table 1 summarizes the number of halos, the halo CME abundance, and the percentage changes during the first 49 months in each SC. In SC 23, there were 100 halos. There was a 4-month data gap in SC 23 (3 months in 1998 and 1 month in 1999), so the 100 halos actually occurred in 45 months with an average rate of ~2.22 halos per month. If halos occurred at this rate during the data gap as well, we expect ~9 additional halos, yielding a total of ~109 halos during the first 49 months of SC 23. The number of halos in SCs 24 and 25 are 26% and 32% higher than the SC 23 number. During the first 49 months, the average sunspot number (<SSN>) decreased by 42% and 27% in SCs 24 and 25, respectively with respect to SC 23. Normalizing the number of halos to <SSN>, we get halo CME abundances of 1.32, 2.87, and 2.38 in SCs 23, 24, and 35 respectively. Clearly, the halo abundance is much higher in SCs 24 and 25, approximately doubling in SCs 24 (117% increase) and 25 (80% increase). Furthermore, the SC 25 halo abundance is in between SCs 23 and 24 but closer to SC 24.

b. Halo CME source locations

Figure 2 plots the heliographic coordinates of the source regions of the halo CMEs in SCs 23-25. Most halo CMEs originate from the latitude range 15º-30º in each hemisphere, which corresponds to the active region belt. This is because large amounts of free energy can be stored in the magnetic regions in the active region belt that can power the halo CMEs. There are no major differences in the latitudinal distributions in the three cycles. However, we see significant differences in the longitudinal distributions, which are much wider in SCs 24 and 25 than in SC 23. For example, the SC 23 data points (red) are generally concentrated close to the disk center, while the SC 24 (blue) and SC 25 (green) data points can be found in almost all longitudes. Halos originating from large central meridian distance are an indication that CMEs expand more in weaker cycles and hence increases their chance of becoming a halo (Gopalswamy et al. 2020b).

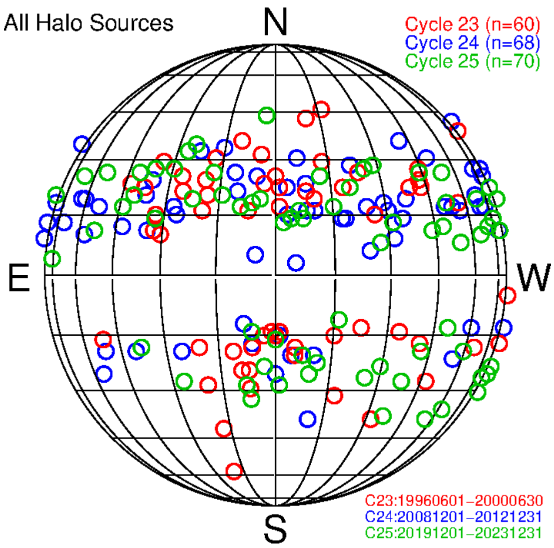

Figure 2. *Sources of halo CMEs during the first 49 months in SCs 23-25, distinguishing the cycles by different colors as indicated in the plot. No correction is made for the B0-angle of the source locations.*

Table 1. *Number of halos in the first 49 months of SCs 23-25 and <SSN>*

	SC 23	SC 24	SC25
Total number of halos	109	137 (+26%)	144 (+32%)
<SSN>	82.7	47.8 (-42%)	60.5 (-27%)
#halos/<SSN>	1.32	2.87 (+117%)	2.38 (+80%)

Figure 3 shows halo CMEs originating close to the limb in the three SCs. Here we have also included CMEs that originated slightly behind the limb (within 30º). There were only 6 limb halos in SC 23. In SC 24, there were 28 limb halos, about 5 times more than the number in SC 23. In SC 25, there were 20 limb halos, which is about 3 times the number in SC 23. Here also, we see that the strongest cycle has the lowest number and the weakest cycle has the largest number of limb halos. If we consider just the frontside events, there were 4, 17, and 15 limb halos in SCs 23, 24, and 25, respectively. This means, only ~7% (or 4/60) of SC 23 halos were at CMD >60º, which is much smaller than the 25% (17/68) in SC 24 and 21.4% (15/70) in SC 25. Once again, SCs 23 and 24 represent extremes, while SC 25 represents intermediate cases but closer to the SC 24 events.

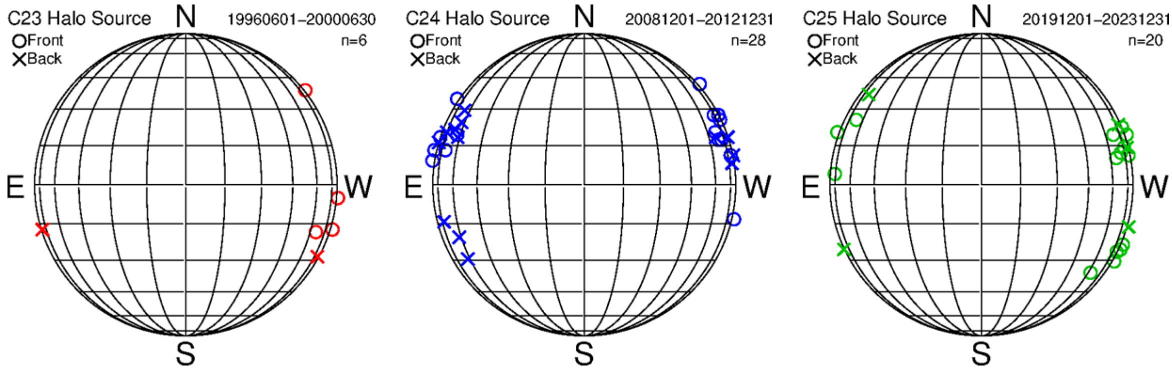

Figure 3. *Sources of halo CMEs during the first 49 months in SCs 23-25, distinguishing the cycles by different colors as indicated in the plot. No correction is made for the B0-angle of the source locations. Backside and frontside halos are indicated by crosses and circles, respectively.*

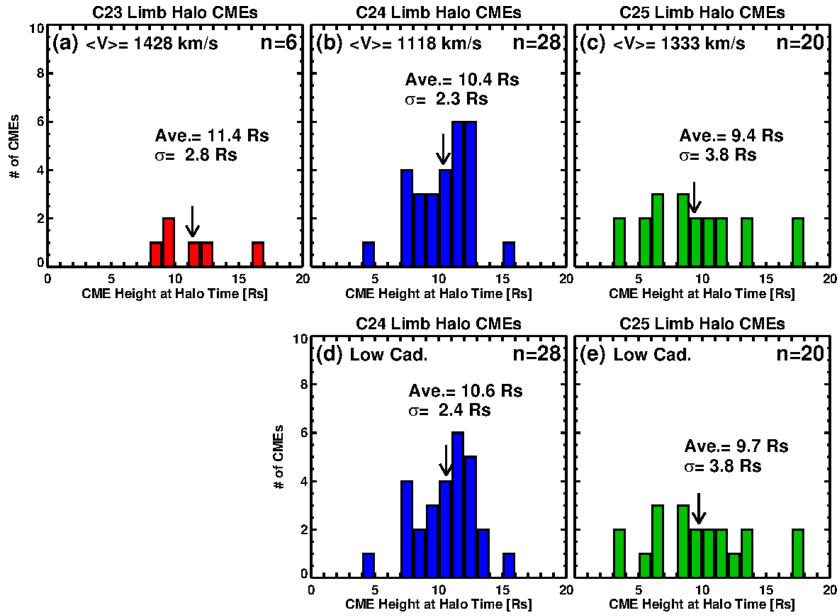

Figure 4. *Halo height distributions obtained from limb halos observed during the first 49 months in SCs 23-25. Halos in Fig. 3 are used for computing the halo heights. The mean (Ave.) and standard deviation (σ) of the distributions are given for each distribution. Also shown are the average speeds of the limb halos.*

c. Height of halo formation

The large number of halo CMEs originating close to the limb were used to determine the height attained by CMEs before becoming a halo (Gopalswamy et al. 2020b). This height, called halo height, was found to be smaller for the weaker SC 24 than for SC 23. This suggests that halos formed closer to the Sun at lower speeds in SC 24, another indication of the backreaction of the weak heliosphere on CMEs. In our previous study we used halos from the first 3 years of each cycle, so the sample sizes were small (Gopalswamy et al. 2023). Here we use an additional 12 months of data, increasing the sample size. We see a similar pattern when the halo heights for the first 49 months are compared in SCs 23-25: halo heights are smaller in SCs 24 and 25 than in SC 23. Furthermore, the average speed of limb halos is the highest in SC 23, followed by SC 25 and SC 24. Here also, SC 25 speed is intermediate between the SC 23 and SC 24 values.

d. Flare sizes in solar cycles 23-25

Figure 5 compares the limb flare sizes during the first 49 months of SCs 23-25. All flares with soft X-ray flare class ≥C3.0 originating within 30º from the limb are considered. All these flares associated with CMEs, but not necessarily halos. The number of flares declined in SCs 24 and 25 with respect to SC 23, but the reduction is not to the same extent as the SSN. When normalized to <SSN>, the number of flares become 2.19, 2.47, 2.51, respectively in SCs 23-25. Interestingly, these values are close to each other unlike the number of halos normalized to <SSN>. Furthermore, the average flare sizes are about the same in the three cycles. These observations suggest that the flares are not affected by the heliospheric state because the flare structures are anchored to the Sun while the CMEs propagate into the heliosphere and face the backreaction.

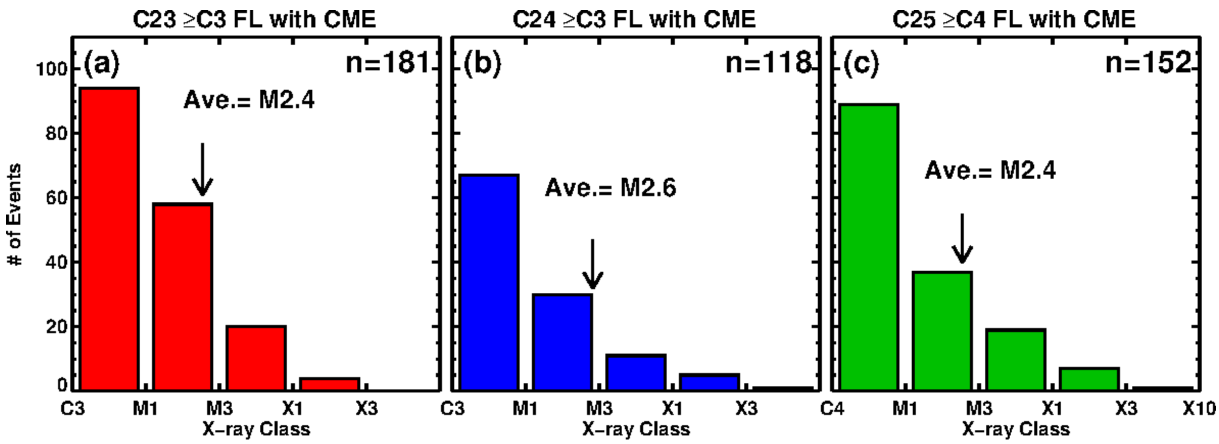

Figure 5. *Distributions of soft X-ray flare sizes reported by NOAA's Space Weather Prediction Center in SCs 23-25. Only flares associated with CMEs are considered. The means of the distributions are shown on the plots (Ave., pointed by arrows). For Cycle 25, ≥C4.0 flares are considered as opposed to ≥C3 flares in SCs 23 and 24. This is because, of rescaling of GOES data, which makes C4 level in SC 25 equivalent to C3 class to be on par with SC s 23 and 24. Details can be found in https://hesperia.gsfc.nasa.gov/goes/goes.html.*

e. Comparison of the number of intense space weather events

Earlier studies indicated that the number of intense space weather events declined significantly in SC 24 relative to SC 23, more than the decline in SSN (Gopalswamy et al. 2014; 2015b, c). Here we compare the intense space weather events during the first 49 months in SCs 23-25 (see Table 2). Intense space weather events we consider are ground level enhancement (GLE) in solar energetic particle events and intense geomagnetic storms (Dst ≤ -100 nT). The decline of intense space weather events is much steeper than that of <SSN>. The explanation for the reduction in the number of GLE events has been attributed to the reduction in ambient magnetic field strength in weaker cycles (Gopalswamy et al. 2014) because the acceleration efficiency is proportional to the ambient field strength. The geomagnetic storms are caused by southward component of the magnetic field in the CME sheath and/or in the magnetic cloud. The anomalous expansion dilutes the magnetic content of the CME and hence results in weaker storms (Gopalswamy et al. 2015c; Yermolaev et al. 2022).

Table 2*. Intense space weather events during the first 49 months of SCs 23-25*

Parameter	SC 23	SC 24	SC 25
Dst ≤ -100 nT	26	9 (-65%)	6 (-77%)
GLEs	4	1 (-75%)	1 (-75%)
SSN	82.7	47.8 (-42%)	60.5 (-27%)

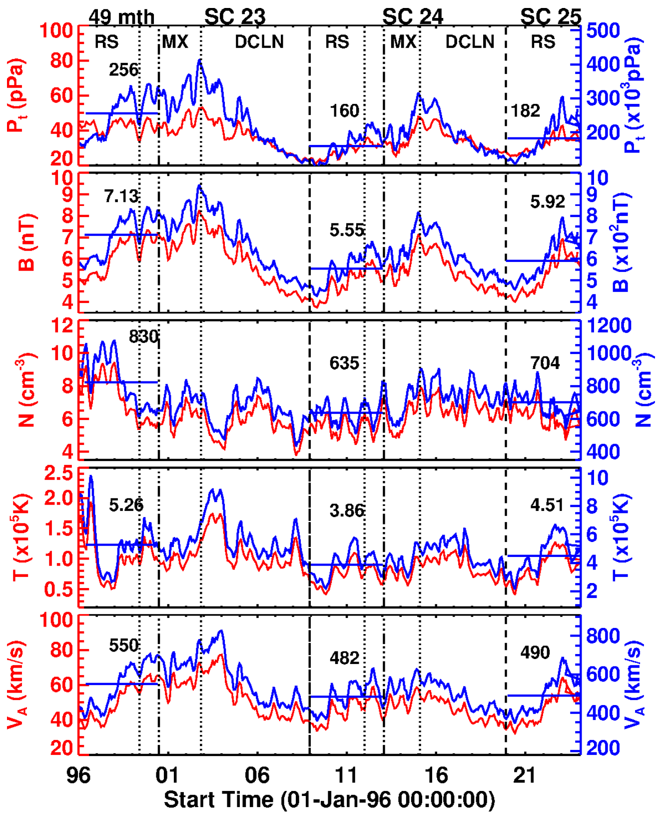

Figure 6. *Total pressure (Pt), magnetic field magnitude (B), proton density (N), proton temperature (T), and the Alfvén speed (V_A) measured at 1 au are plotted in red. The same parameters extrapolated 20 Rs are shown in blue. The horizontal bars denote the average values over the first 49 months. The rise (RS) maximum (MX) and declining (DCLN) phases of the SCs are marked. All parameters are monthly averages obtained from NASA's OMNI web (http://omniweb.gsfc.nasa.gov).*

Heliospheric State

The weak state of the heliosphere referred to in the previous sections can be confirmed from actual observations of the heliosphere at 1 au using in-situ observations of the solar wind plasma and magnetic field. Figure 6 shows several solar wind parameters obtained from NASA's OMNI web for the period 1996 to end of 2023. Solar cycle variation is evident in all quantities related to solar wind magnetic field (total pressure, magnetic field strength, Alfven speed) because ultimately the magnetic field is related to the solar magnetic fields emerging from beneath the solar surface and filling the heliosphere. All parameters show reduction in SCs 24 and 25 with respect to SC 23. The largest reduction is in the total pressure: 38% in SC 24 and 29% in SC 25. The reduction in SC 25 is smaller in all parameters than in SC 24. This implies that SC 25 is slightly stronger than SC 24, but weaker than SC 23, consistent with the pattern seen in halo CME properties in the three cycles.

Table 3. Percentage of reduction of solar wind parameters in SCs 24 and 25 relative to SC 23

Parameter	SC 24	SC 25
Total Pressure	38%	29%
Magnetic Field	22%	17%
Density	23%	15%
Temperature	27%	14%
Alfven speed	12%	11%

Summary

Halo CMEs represent an energetic subset of CMEs that have above average speed and width. CMEs expand sufficiently so brightness enhancement appears all around the occulting disk in sky-plane projection. The brightness enhancement is most often caused by the CME-driven shock. We compared the number of halo CMEs observed during the first ~4 years in solar cycles 23-25 with the aim to see if the strength of solar cycle 25 can be assessed relative to the strengths of solar cycles 23 and 24. The strengths of cycles 23 and 24 have been reported as 180 and 113, respectively. The predicted strength of cycle 25 varies from about half to twice the strength of cycle 24. However, predictions based on polar magnetic field proxies indicate a strength of 136, which is intermediate between the strengths of cycles 23 and 24 (Nandy 2021). Our study is consistent with these precursor-based predictions. The main conclusions of this study are:

1. The halo CME abundance is larger cycles 24 and 25 relative to SC 23: The number of halo CMEs normalized to the average sunspot number during the first 49 months of solar cycles 23, 24, and 25 are 1.32, 2.87, and 2.38, respectively.
2. The halo CME source locations are widely distributed on the solar disk in cycles 24 and 25 compared to cycle 23, resulting in relatively large number of limb halos in cycles 24 and 25: only ~7% of SC 23 halos are at CMD >60º compared to 25% in SC 24 and 21.4% in SC 25.
3. Halo formation heights of CMEs in cycles 24 and 25 are similar but smaller than that in cycle 23.
4. The average speed of limb halos is 1428 km/s, 1118 km/s, and 1333 km/s in cycles 23, 24, and 25, respectively indicating once again that cycle 25 values are in between those of cycles 23 and 24.
5. The soft X-ray flare size distributions are about the same in the three cycles. The drop in the number of flares in cycles 24 and 25 is slightly smaller than the reduction in sunspot number.

The flare numbers normalized to the sunspot number are similar indicating that the backreaction of the heliospheric pressure does not affect the flares.

6. Solar wind parameters measured at 1 au confirm the weak state of the heliosphere in all parameters involving solar wind magnetic field strength, the primary one being the total pressure confirming the backreaction of the heliosphere on CMEs leading to higher halo abundance.

Acknowledgments. Work supported by NASA's LWS program and the STEREO project.

References

Brueckner, G.E., Howard, R.A., Koomen, M.J., Korendyke, C.M., Michels, D.J., Moses, J.D., Socker, D.G., Dere, K.P., Lamy, P.L., Llebaria, A. et al. (1995). The Large Angle Spectroscopic Coronagraph (LASCO). Solar Physics, 162 (1-2), pp. 357–402. https://doi.org/10.1007/bf00733434

Dagnew, F.K., Gopalswamy, N., Tessema, S.B., Akiyama, S., Yashiro, S. and Tesfu, T.Y. (2020a). Intercycle and intracycle variation of halo CME rate obtained from SOHO/LASCO observations. The Astrophysical Journal, 903(2), p.118. https://doi.org/10.3847/1538-4357/abb887

Dagnew, F.K., Gopalswamy, N., Tessema, S.B., (2020b). A comparison of CME expansion speeds between solar cycles 23 and 24. Journal of Physics: Conference Series, 1620(1), pp.012003–012003. http://10.1088/1742-6596/1620/1/012003

Dagnew, F.K., Gopalswamy, N., Tessema, S.B., Akiyama, S. and Yashiro, S. (2022). Effect of the heliospheric state on CME evolution. The Astrophysical Journal, 936(2), p.122. https://doi.org/10.3847/1538-4357/ac8744;

Domingo, V., Fleck, B. and Poland, A.I. (1995). The SOHO mission: An overview. Solar Physics, 162(1-2), pp.1–37. https://doi.org/10.1007/bf00733425

Gopalswamy, N. (2009). Halo coronal mass ejections and geomagnetic storms. Earth, Planets and Space, 61(5), pp.595–597. https://doi.org/10.1186/bf03352930

Gopalswamy, N. (2022). The Sun and Space Weather. Atmosphere, 13(11), p.1781. https://doi.org/10.3390/atmos13111781

Gopalswamy, N., Yashiro, S., Michalek, G., Stenborg, G., Vourlidas, A., Freeland, S. and Howard, R (2009b). The SOHO/LASCO CME Catalog. Earth, Moon, and Planets, 104(1-4), pp.295–313. https://doi.org/10.1007/s11038-008-9282-7

Gopalswamy, N., Yashiro, S., Michalek, G., Xie, H., Mäkelä, P., Vourlidas, A. and Howard, R. (2010). A catalog of halo coronal mass ejections from SOHO. 5(1), pp.7–16. http://newserver.stil.bas.bg/SUNGEO/00SGArhiv/SG_v5_No1_2010-pp-7-16.pdf

Gopalswamy, N., Akiyama, S., Yashiro, S., Xie, H., Mäkelä, P. and Michalek, G. (2014). Anomalous expansion of coronal mass ejections during solar cycle 24 and its space weather implications. Geophysical Research Letters, 41(8), PP.2673-2680, https://doi.org/10.2014- g1059858

Gopalswamy, N., Xie, H., Akiyama, S., Mäkelä, P., Yashiro, S. and Michalek, G. (2015a). The peculiar behavior of halo coronal mass ejections in solar cycle 24. The Astrophysical Journal, 804(1), p.L23. https://doi.org/10.1088/2041-8205/804/1/l23

Gopalswamy, N., Yashiro, S., Xie, H., Akiyama, S. and Mäkelä, P. (2015b). Properties and geoeffectiveness of magnetic clouds during solar cycles 23 and 24. Journal of Geophysical Research: Space Physics,120(11), pp.9221–9245. https://doi.org/10.1002/2015-ja021446

Gopalswamy, N., Akiyama, S., Yashiro, S., Xie, H., Mäkelä, P. and Michalek, G. (2015c). The mild space weather in solar cycle 24. arXiv.org, https://doi.org/10.48550/arXiv- .1508.01603

Gopalswamy, N., Akiyama, S., & Yashiro, S. (2020a). The state of the heliosphere revealed by limb-halo coronal mass ejections in solar cycles 23 and 24. The Astrophysical Journal, 897(1), pp.L1–L1. https://doi.org/10.3847/2041-8213/ab9b7b

Gopalswamy, N., Akiyama, S., Yashiro, S., Michalek, G., Xie, H. and Mäkelä, P. (2020b). Effect of the weakened heliosphere in solar cycle 24 on the properties of coronal mass ejections. Journal of Physics: Conference Series, 1620(1), P012005. https://doi.org/10.1088/1742-6596/1620/1/012005

Gopalswamy, N., Mäkelä, P., Yashiro, S., Akiyama, S. and Xie, H. (2022). Solar activity and space weather. Journal of Physics: Conference Series, 2214(1), p.012021.https://doi.org/10.1088/1742-6596/2214/1/012021

Howard, R.A., Michels, D.J., Sheeley, N.R., Jr. and Koomen, M.J. (1982). The observation of a coronal transient directed at Earth. The Astrophysical Journal, 263, pp. L101–L104. https://doi.org/10.1086/183932

Howard, R.A., Sheeley, N.R., Koomen, M.J. and Michels, D.J. (1985). Coronal mass ejections: 1979–1981. Journal of Geophysical Research, 90(A9), p.8173. https://doi.org/10.1029/ja090ia09p08173

McComas, D.J., Angold, N.G., Elliott, H.A., Livadiotis, G., Schwadron, N.A., Skoug, R.M. and Smith, C.D. (2013). Weakest solar wind of the space age and the current ‘mini’ solar maximum. The Astrophysical Journal, 779(1), pp.2–2. https://doi.org/10.1088/0004-637x/779/1/2

Michalek, G., Gopalswamy, N. and Yashiro, S. (2019). On the coronal mass ejection detection rate during solar cycles 23 and 24. The Astrophysical Journal, 880(1), p.51. https://doi.org/10.3847/1538-4357/ab26a7

Nandy, D. (2021). Progress in solar cycle predictions: sunspot cycles 24–25 in perspective. Solar Physics, 296(3). https://doi.org/10.1007/s11207-021-01797-2

Petrie, G. (2015). On the enhanced coronal mass ejection detection rate since the solar cycle 23 polar field reversal. The Astrophysical Journal, 812(1), pp.74–74. https://doi.org/10.1088/0004-637x/812/1/74

Yashiro, S., Gopalswamy, N., Michalek, G., St. Cyr, O. C. Plunkett, S. P. Rich, N. B. Howard, R. A. (2004). A catalog of white light coronal mass ejections observed by the SOHO spacecraft. Journal of Geophysical Research, 109(A7). https://doi.org/10.1029/2003ja010282

Yermolaev, Y.I., Lodkina, I.G., Khokhlachev, A.A. and Yermolaev, M.Y. (2022). Peculiarities of the heliospheric state and the solar-wind/magnetosphere coupling in the era of weakened solar activity. Universe, 8(10), p.495. https://doi.org/10.3390/universe8100495

Zhang, J., Temmer, M., Gopalswamy, N., Malandraki, O., Nitta, N.V., Patsourakos, S., Shen, F., Vršnak, B., Wang, Y., Webb, D., Desai, M.I., (2021). Earth-affecting solar transients: a review of progresses in solar cycle 24. Progress in Earth and Planetary Science, 8(1). https://doi.org/10.1186/s40645-021-00426-7

Zhao, X.P. and Webb, D. F. (2003). Source regions and storm effectiveness of frontside full halo coronal mass ejections. Journal of Geophysical Research, 108(A6). https://doi.org/10.1029/2002ja009606